rather large for $g_s^2 \sim 1$ and its vector element is rather insensitive to g_v^2. A similar criticism of a $^1G_4$ based on OPEC has already been made by the Yale group themselves on the grounds of a comparison with experiment.[8] It is interesting to speculate that here OPEC should be based on ϵ_4, since the behavior of this phase shift is quite unusual in this model. Its scalar-meson matrix element (for $g_s^2=1$) is very small at 310 MeV, and, in fact, disappears in the nonrelativistic limit. Its vector-meson element, though larger than the scalar (for $g_s^2=g_v^2$), is also small because of the short range of the ρ and ω; therefore, $\alpha(\epsilon_4)$ should be quite close to its OPEC value. The table shows this insensitivity to g_s^2 and g_v^2 values.

The $^3H_4$ phase shift shows the normal attenuation of scalar and vector matrix elements at high l; it will probably be close to its OPEC value if the ratios of g_s^2 to g_v^2 are similar to those shown in the table. Just like all the matrix elements considered, the vector contribution is opposite in sign to that of the scalar, so that, for instance, for $M_s=3\,\mu$, $^3H_4$ is equal to $(^3H_4)_{\text{OPEC}}$ if

$$g_s^2=0.0370\,g_v^2$$

and greater than OPEC for larger g_s^2.

[8] G. Breit, M. H. Hull, Jr., K. E. Lassila, and H. N. Ruppel, Phys. Rev. Letters **5**, 274 (1960) and Proc. Natl. Acad. Sci. **46**, 1649 (1960).

As for the ^3F and $^1G_4$ waves, one set of values from low l work,[1] i.e., $g_s^2(M_s=4\,\mu)=16$ and $g_v^2=34$, gives $\alpha(^3F_4)=0.125$. This result agrees with the table in asserting that the phase-shift solutions 1, 5, and 6 give too small a $^3F_4$ phase shift. The modified phase-shift analysis would be a test of this conjecture.

The conclusions given here would be modified slightly by the inclusion of the $J=0^-$, $T=0$ particle of mass $\simeq 4\,\mu$, the η meson. This particle increases slightly the absolute value of the $^1G_4$ and $^3F_4$ phase shifts, and decreases that of the $^3F_3$ wave; the resultant g_s^2 and g_v^2 would be somewhat less than those given in the table.

Further modifications would involve the inclusion of a derivative-coupling vector term. The Dirac term given, however, seems to be by far the most important in p-p scattering, consonant with the apparent dominance of ω exchange in the nucleon form factor results.[1]

ACKNOWLEDGMENT

This work developed from a previous collaboration with Dr. R. Bryan. The author wishes to thank him for all his advice and comments. Part of the calculation was done at the University of California, Los Angeles, with support from the National Science Foundation.

Thanks are also due to Dr. D. Wong for valuable comments.

PHYSICAL REVIEW VOLUME 130, NUMBER 4 15 MAY 1963

Branching Ratios of Reactions of π^- Mesons Stopped in Hydrogen and Deuterium*

JAMES W. RYAN†
Lawrence Radiation Laboratory, University of California, Berkeley, California
(Received 7 January 1963)

We measure the Panofsky ratio $P=\omega(\pi^-+p\rightarrow\pi^0+n)/\omega(\pi^-+p\rightarrow\gamma+n)$ and the branching ratio $S=\omega(\pi^-+d\rightarrow n+n)/\omega(\pi^-+d\rightarrow\gamma+n+n)$ by stopping π^- mesons in liquid hydrogen and liquid deuterium and detecting the γ rays produced. A high-resolution γ-ray spectrometer of the 180-deg-focusing type is employed. Sixty-six Geiger tubes and nine scintillation counters are used in the spectrometer to define the electron-positron orbits, providing an intrinsic instrument resolution of 0.8%. The values we obtain for the branching ratios are $P=1.51\pm0.04$ and $S=3.16\pm0.12$. This value for P is in good agreement with that obtained in previous measurements, while the value for S is significantly larger than previous results. With regard to the conventional phenomenological analysis of S-wave pion physics, the Panofsky ratio is in good agreement, whereas the value obtained in this experiment for the branching ratio S is considerably larger than predicted.

I. INTRODUCTION

WHEN a π^- meson comes to rest ($\beta<0.01$) in liquid hydrogen, nuclear capture occurs in approximately 10^{-12} sec through one of the following channels:

$$\pi^-+p\rightarrow\pi^0+n, \tag{1}$$

$$\pi^-+p\rightarrow\gamma+n, \tag{2}$$

or

$$\pi^-+p\rightarrow e^-+e^++n. \tag{3}$$

Reaction (1), mesonic capture, produces a 0.41-MeV neutron and a π^0 meson with $\beta=0.21$. The lifetime for decay of the π^0 is approximately 2×10^{-16} seconds and leads to one of the following final states:

$$n+\gamma+\gamma, \tag{1a}$$

$$n+\gamma+e^++e^-, \tag{1b}$$

or

$$n+e^++e^-+e^++e^-. \tag{1c}$$

* Work done under the auspices of the U. S. Atomic Energy Commission.

† Present address: University of Rochester, Department of Physics, Rochester, New York.

The branching ratio of the internal-conversion reaction (1b) to reaction (1a) has been calculated by Joseph[1] to be 0.00710. Due to motion of the π^0, the γ rays emitted are uniformly distributed in energy between 54.75 and 83.25 MeV.

Reaction (2), radiative capture, yields an 8.9-MeV neutron and a monoenergetic γ ray of 129.4 MeV. Reaction (3) corresponds to internal conversion of this γ ray. The branching ratio (3)/(2) is calculated as 0.01196.[1]

The Panofsky ratio P is generally defined as the branching ratio between the mesonic-capture and the radiative-capture reaction rates, excluding the low-yield internal-conversion processes. However, we include here the contribution from these processes and define P in the same manner as Cocconi *et al.*[2] as:

$$P=\frac{(1)}{(2)+(3)}=\frac{(1a)+(1b)}{(2)+(3)}. \tag{4}$$

When π^- mesons come to rest in deuterium, the following nuclear reactions occur:

$$\pi^-+d\rightarrow n+n, \tag{5}$$

$$\pi^-+d\rightarrow n+n+\gamma, \tag{6}$$

and

$$\pi^-+d\rightarrow n+n+\pi^0. \tag{7}$$

Reaction (5) yields monoenergetic neutrons of 67.5 MeV. The radiative-capture reaction (6) produces γ rays with a distribution of energies ranging from 0 to 131.5 MeV that is peaked near the high-energy end as a result of the n-n interaction.

In their original experiment, Panofsky *et al.*,[3] stopped π^- mesons in both hydrogen and deuterium and detected the nuclear γ rays with a pair spectrometer. In addition to measuring the Panofsky ratio, they also obtained values for the deuterium ratios S and K, defined as

$$S=\omega(\pi^-+d\rightarrow n+n)/\omega(\pi^-+d\rightarrow n+n+\gamma), \tag{8}$$

and

$$K=\omega(\pi^-+d\rightarrow n+n+\pi^0)/\omega(\pi^-+d\rightarrow n+n+\gamma). \tag{9}$$

After this initial work, several additional measurements of the Panofsky ratio were published.[2,4–11] (These are listed in Table I together with previous measurements of S and K.)[3,12–14]

Anderson and Fermi[15] first pointed out that the Panofsky ratio serves as a connecting link between reactions in pion-nucleon scattering and pion photoproduction. Brueckner, Serber, and Watson[16] later showed how the deuterium ratio S connects reactions involving pion production in nucleon-nucleon collisions with these other interactions. These connections provide a means of checking the internal consistency of a large body of knowledge in low-energy pion physics. If it is assumed for the bound-state reactions that nuclear capture occurs predominantly from S states, the ratios P and S can be expressed as

$$P=\frac{4\pi}{9R}\frac{v_0}{q}\frac{(1+\mu/\mathfrak{M})^2}{(1+\mu/2\mathfrak{M})^2}\frac{(\delta_3-\delta_1)^2}{\sigma(\gamma+p\rightarrow n^++n)}, \tag{10}$$

and

$$S=\frac{1}{3\tau' R}\frac{1+\mu/\mathfrak{M}}{1+\mu/2\mathfrak{M}}\frac{Mq}{q'}\frac{\sigma(p+p\rightarrow\pi^++d)}{\sigma(\gamma+p\rightarrow\pi^++n)}. \tag{11}$$

Here, μ and $\mathfrak{M}$ are the pion and nucleon rest masses, δ_3 and δ_1 are the S-wave-scattering phase shifts for isotopic-spin states 3/2 and 1/2, respectively, v_0 is the π^0 velocity relative to the neutron for the charge-exchange reaction in hydrogen, while q and q' are incident c.m. π^- momenta for the reactions in hydrogen and deuterium. Also, we have $\tau'=\tau|\phi(0)|^2/|\phi'(0)|^2$, where $\phi(0)$ and $\phi'(0)$ are the wave functions for the respective hydrogen and deuterium mesonic-atom states from which capture occurs, both evaluated at the position of the nucleus. Here $\tau=\omega(\pi^-+d\rightarrow\gamma+2n)/\omega(\pi^-+p\rightarrow\gamma+n)$, where the transition rates are for bound-state captures and $R=\sigma(\gamma+n\rightarrow\pi^-+p)/\sigma(\gamma+p\rightarrow\pi^++n)$, where the ratio is evaluated at threshold. Equations (10) and (11) have been discussed previously.[5,6,15,16]

Since Anderson and Fermi first published their paper, discrepancies between the calculated Panofsky ratio, Eq. (10), and the measured value have stimulated a large amount of experimental and theoretical work. Several different suggestions were offered to explain these discrepancies, including violation of charge independence in the pion-nucleon system[17] and even the existence of a new particle.[18] However, due largely to the theoretical work of Baldin,[18] Cini, Gatto, Gold-

[1] D. W. Joseph, Nuovo Cimento **16**, 997 (1960).
[2] V. T. Cocconi, T. Tazzini, G. Fidecaro, M. Legros, N. H. Lipman, and A. W. Merrison, Nuovo Cimento **22**, 494 (1961).
[3] W. K. H. Panofsky, R. L. Aamodt, and J. Hadley, Phys. Rev. **81**, 565 (1951).
[4] C. P. Sargent, R. Cornelius, M. Rinehart, L. M. Lederman, and K. Rogers, Phys. Rev. **98**, 1349 (1955).
[5] J. M. Cassels, G. Fidecaro, A. Wetherell, and J. R. Wormald, Proc. Phys. Soc. (London) **A70**, 405 (1957).
[6] J. Fischer, R. March, and L. Marshall, Phys. Rev. **109**, 533 (1958).
[7] J. Kuehner, A. W. Merrison, and S. Tornabene, Proc. Phys. Soc. (London) **73**, 545 (1959).
[8] (a) L. Koller and A. M. Sachs, Phys. Rev. **116**, 760 (1959); (b) A. F. Dunaitsev, V. S. Panteuv, Yu. D. Prokoshkin, Fang Syoa-Wei, and M. N. Khachaturyan in *Proceedings of the 1960 Annual International Conference on High-Energy Physics, Rochester*, edited by E. C. G. Sudarshan, J. H. Tinlot, and A. C. Melissions (Interscience Publishers, Inc., New York, 1960), p. 181.
[9] M. Derrick, J. Tetkovich, T. Fields and J. Deahl, Phys. Rev. **120**, 1022 (1960).
[10] N. P. Samios, Phys. Rev. Letters **4**, 470 (1960).
[11] D. P. Jones, P. G. Murphy, P. L. O'Neill, and J. R. Wormald, Proc. Phys. Soc. (London) **A77**, 77 (1961).
[12] W. Chinowsky and J. Steinberger, Phys. Rev. **95**, 1561 (1954).
[13] W. Chinowsky and J. Steinberger, Phys. Rev. **100**, 1476 (1955).
[14] J. A. Kuehner, A. W. Merrison, and S. Tornabene, Proc. Phys. Soc. (London) **73**, 551 (1958).
[15] H. L. Anderson and E. Fermi, Phys. Rev. **86**, 794 (1952).
[16] K. A. Brueckner, R. Serber, and K. M. Watson, Phys. Rev. **81**, 575 (1951).
[17] H. P. Noyes, Phys. Rev. **101**, 320 (1956).
[18] A. Baldin, Nuovo Cimento **8**, 569 (1958).

TABLE I. Measurements of the ratios P, K, and S.[a]

Experimenter	Reference	Method	Ratio
Panofsky *et al.*	3	Pair spectrometer	$P=0.94\pm0.30$ $S=2.36\pm0.74$ $K=0.003\pm0.073$
Sargent *et al.*	4	Cloud chamber	$P=1.10\pm0.50$
Cassels *et al.*	5	Total absorption Čerenkov detector	$P=1.50\pm0.15$
Fischer *et al.*	6	Total absorption Čerenkov detector	$P=1.87\pm0.10$
Kuehner *et al.*	7	Pair spectrometer	$P=1.60\pm0.17$
Koller	8(a)	Total absorption Čerenkov detector	$P=1.46\pm0.10$
Dunaitsev *et al.*	8(b)	γ-γ Coincidence	$P=1.40\pm0.08$
Derrick *et al.*	9	Bubble chamber	$P=1.47\pm0.10$
Samios	10	Bubble chamber	$P=1.62\pm0.06$
Jones *et al.*	11	Total absorption Čerenkov detector	$P=1.56\pm0.05$
Cocconi *et al.*	2	Total absorption NaI detector	$P=1.533\pm0.021$
Chinowsky and Steinberger	12	Counter detection of both reactions	$S=1.5\pm0.8$ $K=0.0034\pm0.0043$
Chinowsky and Steinberger	13		
Kuehner *et al.*	14	Pair spectrometer	$S=2.36\pm0.36$
This experiment, Measurement I		Pair spectrometer	$P=1.490\pm0.050$ $S=3.16\pm0.12$
Measurement II		Pair spectrometer	$P=1.543\pm0.063$
Average	...	...	$P=1.51\pm0.04$
Weighted average	...	...	$P=1.53\pm0.02$ $S=3.05\pm0.11$
Calculated values[b]	...	...	$P=1.55\pm0.24$ $S=1.58\pm0.36$

[a] See text for definition of P, K, and S.
[b] Calculated values based upon references: $\delta_3-\delta_1=(0.245\pm0.007)q$ (reference 20); $\sigma(\gamma+p\rightarrow\pi^++n)=(0.19\pm0.02)q\times10^{-27}$ cm² [W. P. Swanson, Lawrence Radiation Laboratory Report, UCRL-9194 (1960) (unpublished)]; $\sigma(p+p\rightarrow\pi^++d)=(1.38\pm0.15)q'\times10^{-28}$ cm² [F. S. Crawford and M. L. Stevenson, Phys. Rev. **97**, 1305 (1955)]; $R=1.33\pm0.14$ (reference 20); $\tau=0.83\pm0.08$ (reference 21).

wasser, and Ruderman,[19] and Hamilton and Woodcock[20] plus more precise determinations of the Panofsky ratio, no serious discrepancies now seem to exist.

The chain of reactions in deuterium involving the ratio S provides an independent check on the results in hydrogen. Because of the relatively large uncertainties in previous measurements of S and in the ratio τ, this check has not been very useful.

In this experiment, we report on a 3% measurement of both the Panofsky ratio P and the deuterium ratio S. The calculated and measured values of P and S are compared in Table I, using a recent more accurate evaluation[21] of τ.

II. EXPERIMENTAL METHOD

Uncertainty in previous measurements of the Panofsky ratio has been caused by statistics as well as by inadequate resolution of the γ-ray spectra involved. Considering this, and because we also wished to determine the spectrum of γ rays from the deuterium reaction with good resolution, a γ-ray pair spectrometer was selected. The spectrometer is of the 180-deg-focusing type and is discussed in detail in Sec. III.

[19] M. Cini, R. Gatto, E. L. Goldwasser, and M. Ruderman, Nuovo Cimento **10**, 243 (1958).
[20] J. Hamilton and W. S. Woolcock, Phys. Rev. **118**, 291 (1960).
[21] R. Traxler, Lawrence Radiation Laboratory Report UCRL-10417, 1962 (unpublished).

A. Panofsky Ratio

If a large number of π^- mesons stop in hydrogen, the Panofsky ratio is equal to the ratio of the number of mesonic-capture reactions to the number of radiative-capture reactions that occur. Let $N_{\gamma1}$ and $N_{\gamma2}$ be the number of γ rays from each of these reactions, respectively, that strike the converter of the spectrometer. If no losses occur in the target, then the Panofsky ratio can be written as

$$P=N_{\gamma1}/2N_{\gamma2}, \tag{12}$$

where the 2 compensates for the two γ rays produced in the mesonic-capture reaction.

With the present spectrometer, we can measure the Panofsky ratio with optimum efficiency by using two different mean energy settings of the spectrometer, one corresponding to the energy of the radiative-capture γ ray, the other to the midpoint energy of the distribution of mesonic-capture γ rays. For a fixed magnetic-field setting the present spectrometer is capable of detecting the γ rays from both reactions but with reduced efficiency.

We decided to make two independent measurements, one with a single fixed field, the other with two different fields. For the three field settings the converter thicknesses were chosen to equalize scattering losses (see Sec. IIIC). Thereby, an absolute comparison of the γ-ray yield at different magnetic fields for each of the

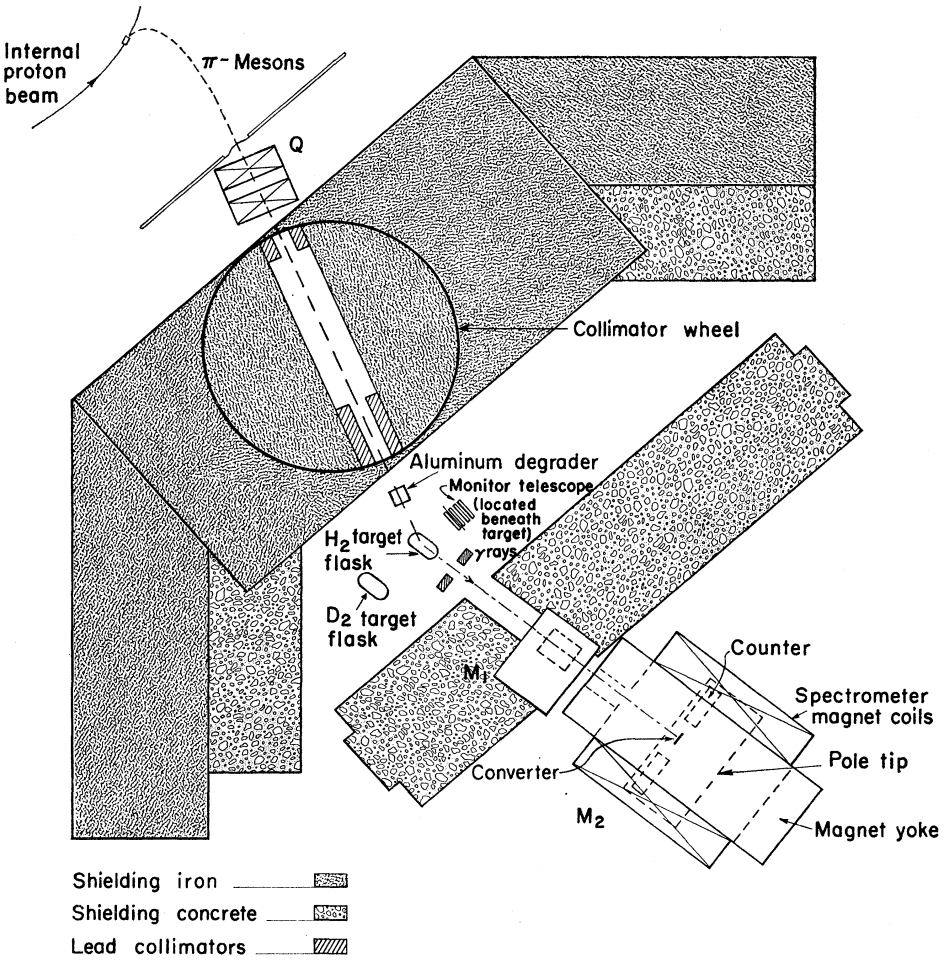

FIG. 1. Equipment setup in the meson-beam cave of the 184-in. cyclotron.

two reactions provided a rigorous check of the pair spectrometer.

B. Deuterium Ratio S

If a large number, N, of π^- mesons stop in hydrogen and the same number stop in deuterium, we can write

$$N=N_1(\pi^-+p\rightarrow\pi^0+n)+N_2(\pi^-+p\rightarrow\gamma+n)$$
$$=N_3(\pi^-+d\rightarrow n+n)+N_4(\pi^-+d\rightarrow n+n+\gamma), \quad (13)$$

where N_1, N_2, N_3, and N_4 are the number of interactions which occur in the respective channels. (The small contributions from internal-conversion processes are neglected.) Since $P=N_1/N_2$, and $S=N_3/N_4$, Eq. (13) can be rearranged to give

$$S=(1+P)\frac{N_2}{N_4}-1. \quad (14)$$

If $N_{\gamma 2}$ and $N_{\gamma 4}$ are the number of γ rays incident on the spectrometer converter from the respective reactions, S can be expressed as

$$S=(1+P)\frac{N_{\gamma 2}}{N_{\gamma 4}}-1. \quad (15)$$

III. EXPERIMENTAL EQUIPMENT

A. Equipment Arrangement

Arrangement of the experimental equipment is shown in Fig. 1. The π^- meson beam is produced in a Be target bombarded in the 184-in. cyclotron. After leaving the vacuum tank through a thin window, the beam passes through an 8-in.-diam quadrupole doublet and an 8-ft-diam iron collimating wheel with a 5-in.-square aperture. The beam is reduced in energy as it passes through an aluminum degrader, the thickness of which is chosen to stop the mesons in the liquid hydrogen or deuterium flask.

A fraction of the γ rays produced by π^- mesons interacting in the liquid-hydrogen pair produce in the converter of the pair spectrometer, M_2, and the resulting electron-positron pairs are detected.

Lead bricks forming a 6-in.-square collimating hole near the hydrogen target shield the converter from view of all portions of the target except the flask. The small magnet M_1 sweeps away charged particles which might otherwise enter the spectrometer entrance channel.

Two separate beam monitoring systems were used.

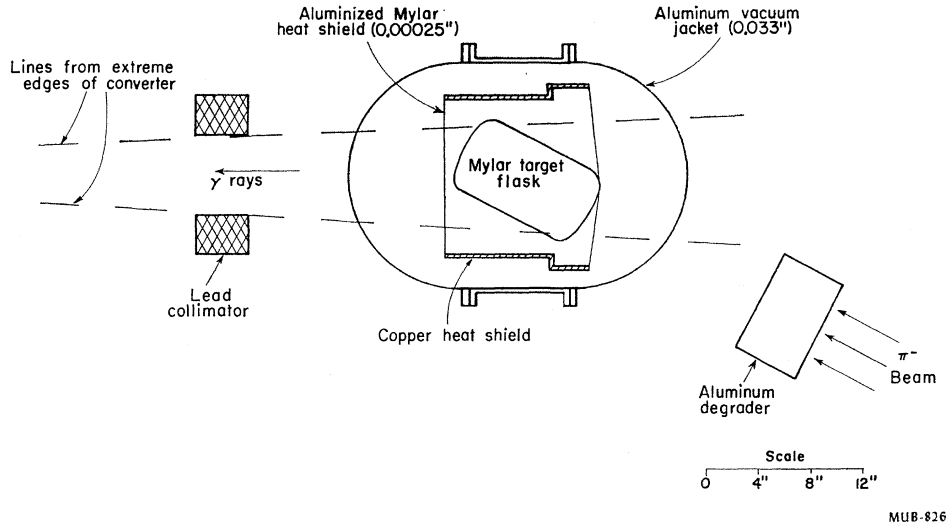

FIG. 2. Diagram showing target and beam configuration.

One, an ion chamber, was located near the cyclotron vacuum tank inside the shielding wall and the ion current was continuously monitored. The other, a γ-ray telescope, was located below the target.

B. Hydrogen and Deuterium Targets

Both hydrogen and deuterium targets were rigidly mounted on a carriage which in turn was suspended on flanged wheels from a support stand and was movable by hand to allow positioning either of the target flasks in the beam path. The maximum error in the relative positioning of the two flasks was 0.250 in.

A schematic diagram showing the target flask, heat shield, and outer vacuum jacket is shown in Fig. 2. Both the hydrogen and deuterium targets are of identical design. The flask is cylindrical in shape with a 6-in. diam and 10-in. average length. It is fabricated from 0.010-in. Mylar.

To guard against contamination of the liquid hydrogen, we transferred the hydrogen from the Dewar flask to the target by using hydrogen gas under pressure.

C. The γ-Ray Pair Spectrometer

A top view of the spectrometer with the upper half of the electromagnet removed is shown in Fig. 3. Gamma rays enter the spectrometer through a 6×7 in. hole in the electromagnet yoke. Converted pairs are turned in a circular path by a uniform magnetic field perpendicular to the plane of the drawing; the pairs are detected at the 180-deg position. An array of 33 Geiger tubes on each side of the converter plus 9 scintillation counters detect the particles and determine the sum of their energies.

The distance between the centers of the detection region on both sides of the converter is 32 in. As will be described later, overlap of the Geiger tubes gives a 0.25-in. channel width. Together, these dimensions define an intrinsic instrument resolution of 0.8%.

1. *General Features of the 180-degree Design*

The principles of the 180-deg pair spectrometer were first discussed by Walker and McDaniel[22] and applied to an instrument with an energy range of 5–40MeV. Later, Kuehner, Merrison and Tornabene[7] used this type of design in a measurement of the Panofsky ratio.

The important characteristics of the 180-deg design are as follows:

(a) The total electron-positron pair energy is proportional to the distance between orbits at the 180-deg position and is independent of the horizontal position of pair creation in the converter.

(b) Horizontal displacements of the pair members at the focus line resulting from their angular displacements at the converter are minimized because of focusing to the first order in the angle.

(c) Vertical displacement of the pair members at the focus line due to multiple scattering in the converter is independent of particle energy, depending only on the converter thickness and magnetic field strength. Therefore, for different magnetic field values the converter thicknesses can be appropriately chosen to equalize scattering losses.

2. *The Magnetic Field*

Because it is mathematically advantageous to use a spectrometer with a uniform magnetic field so that particle orbits are circular arcs, a program of field measurements and shimming of the spectrometer magnet was carried out. The final shim configuration provided a quite uniform field over the range of field strength employed in the experiment. Analysis indicates that the error on the measured ratios resulting from assuming circular orbits is less than 0.2%. To ensure a field constant in time, the magnet-coil current was regulated to better than 5 parts in 10^4.

[22] R. L. Walker and B. D. McDaniel, Phys. Rev. **74**, 315 (1948).

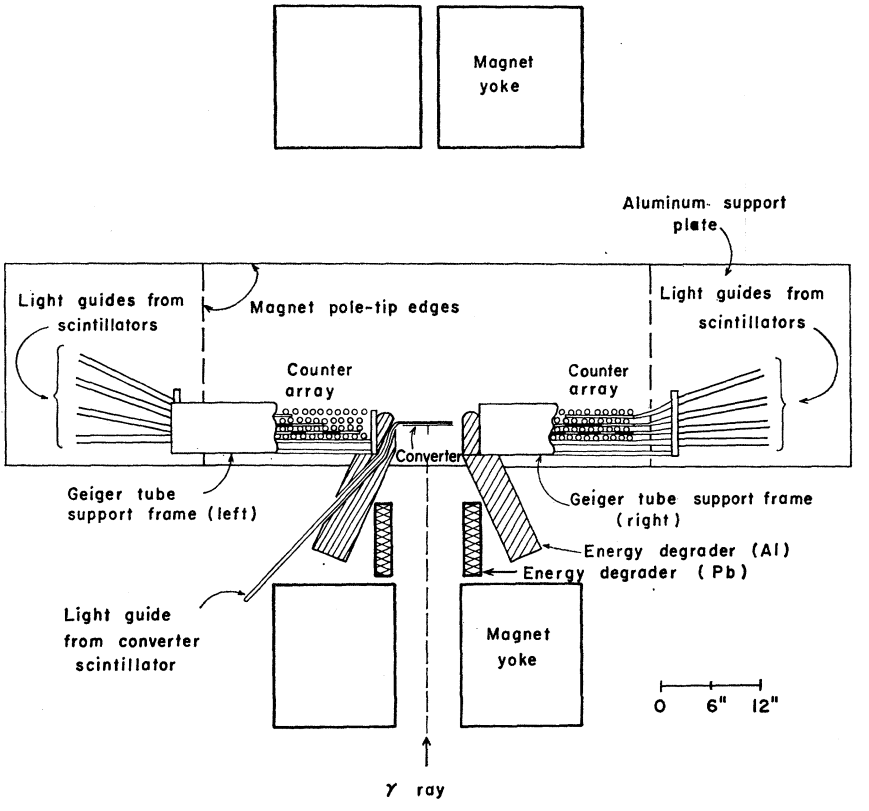

FIG. 3. Top view of spectrometer with upper half of electromagnet yoke removed.

3. *Converters*

The converters were made from lead foil mounted on a 0.060-in. Lucite support plate. Thicknesses of the lead in converter C-1, C-2, and C-3 were 0.2293, 0.4781, and 0.8102 g/cm^2, respectively. Besides the lead and Lucite backing, the converter scintillation counter also forms part of the converter system. However, the effective thickness for pair production in the converter counter is not known. The manner in which the data is treated to account for this is discussed in Sec. VIC.

4. *Counters*

The counter-detection system consisted of 66 Geiger tubes and 9 scintillation counters arranged as shown in Fig. 4. A coincidence between the gate counters scintillators 1, 2-*N*, and 3-*P*) indicates the detection of an electron-positron pair created in the converter. The total energy of the pair is determined by those Geiger tubes and scintillation counters, 4-*N* through 9-*P* which fire in coincidence with the gate counters. The scintillation counters serve as a check on the Geiger-tube system and help to define events when extra Geiger tubes fire.

The Geiger tubes (Victoreen type IB85) are cylindrical in shape with a 0.750-in.-diam outer aluminum shell of thickness 0.007 in. The present tube arrangement has been used previously.[23] By overlapping tubes and requiring a coincidence for the overlap channels, we obtain a channel width of 0.250 in. To increase the active area of the channels, pairs of Geiger tubes are arranged parallel end to end to provide a total active length of nearly 5 in. Vertical overlap is employed to compensate for the reduced efficiency near the tube end. The positions of the tubes are known to within 0.015 in. Identically numbered tubes in Fig. 4 define a pair of parallel tubes which form a part of the same energy channels and are connected electrically to the same lead. These numbers serve to determine the energy of the detected pairs.

Scintillation counter No. 1 is located directly behind the converter and has a thickness of 0.050 in. Counters 2-*N* and 3-*P* are composed of tapered pieces of plastic scintillator and lucite bonded together to form a uniform 0.500-in.-thick strip. The piece of scintillator is from 0.25 to 0.45 in. thick. This design provides uniform phototube pulses and ensures that the detection efficiency was independent of electron energy. Counters 4-*N* through 9-*P* are composed of alternate 0.125-in.-thick strips of lucite and scintillator and form a complete separate system for defining the energy channels, with a resolution of 6%. However, the usefulness of this system is limited as a result of the relatively large efficiency (5 to 10%) for detecting Čerenkov radiation in Lucite strips.

The rms variation in efficiency of the Geiger tubes

[23] K. M. Crowe and R. H. Phillips, Phys. Rev. **96**, 470 (1954).

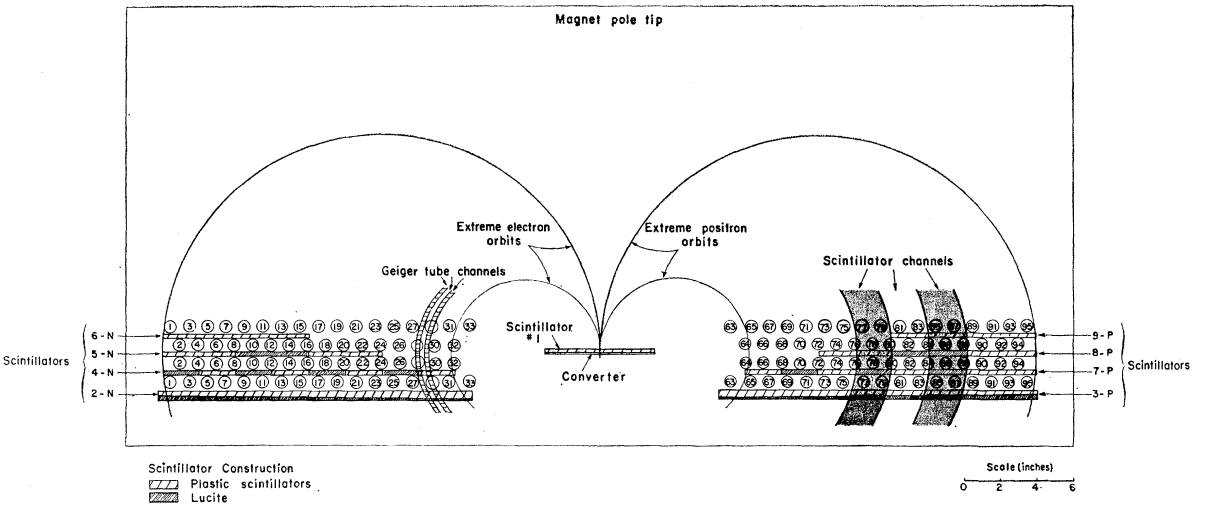

FIG. 4. Schematic drawing showing counter locations and Geiger-tube numbering system.

used in our experiment is approximately 4%. Although calculations indicate that the absolute efficiency should be nearly 100%, the results of our experiment indicate it to be between 85 and 90%; tube-end effects may cause this difference.

By observing which channel-scintillation counters fired when specific Geiger channels fired we determined that the efficiency for each scintillator channel (see Fig. 4) was >97%.

D. Data-Recording System

The data-recording system detects and indicates photographically those channel-defining counters (both Geiger and Scintillation counters) that fire simultaneously with the three gate counters.

A fast coincidence (10 nsec) between the three gate counters generates both a fast and slow output pulse. The fast pulse is put in twofold coincidence with each of the channel-scintillation counters. The output from each of these twofold coincidence circuits is fed into a separate gated "amplifier and pulse generator" unit. Each of the 64 pair of paralleled Geiger tubes is also connected to the input of one of these units.

The slow pulse (5 μsec) generated by the gate-counter coincidence provides a slow coincidence between the gate counters and the channel-defining counters in the "amplifier and pulse generator" units. A neon lamp is located in the output circuit of each unit. These lamps, when fired, indicate coincidence events and are photographically recorded.

IV. EXPERIMENTAL PROCEDURES

Cyclotron runs are made with various combinations of spectrometer converters and magnetic fields as indicated in Table II. Panofsky ratios I and II refer to the two independent measurements performed, as described in Sec. II, one utilizing a fixed magnetic field (II) and the other, two different fields (I). The runs with converter out determine the effect of the converter counter. Additional background measurements not indicated in the table were made with the converter both in and out, but with the hydrogen removed from the flask. To help cancel systematic monitoring and background effects due to cyclotron operation, we performed a large number of individual runs (130), alternating them between the various magnetic-field and converter combinations. During measurement of the deuterium ratio S, runs with the hydrogen and deuterium targets were alternated.

To correct for the difference in stopping power between the liquid hydrogen and deuterium, we measure γ-ray yield vs hydrogen density. Changes in density are made by altering the pressure in the hydrogen flask. The minimum and maximum pressures attained were 3 and 30 psia, corresponding to a change of hydrogen density from 67 to 75 g/liter. Values of density are determined from the hydrogen temperature, which is measured using a copper-constantan thermocouple. One junction is located near the bottom of the hydrogen target, while the reference junction is located in a liquid-nitrogen bath. Voltage measurements were made with a Leed's and Northrup K–2 potentiometer. With this system the temperature could be determined within 0.2 deg.

V. SPECTROMETER RESOLUTION AND DETECTION EFFICIENCY

Assume that a γ ray selected at random from a spectrum with energy distribution $I(E_\gamma)$ is incident on a converter of thickness T. Then the probability that a pair is produced and detected with total energy between

TABLE II. Treatment of measured data.

Measurement	Field	Converter	H_2 or D_2	Relative monitor counts	Total gates	Total events recorded	Events rejected A	B	C	D	Uncertain events	Energy interval $E_A \rightarrow E_B$	Acceptable events Good	Extra	Total (n_d)	N_d
Panofsky ratio I	5538	C-1	H_2	39.43	4954	4851	378	1458	210	11 (high) 6 (low)	11	40.1 to 82.2	2214	563	2777	7358
Panofsky ratio I	5538	out	H_2	16.83	278	251	21	93	11	2 (low)	2	40.1 to 82.2	92	30	122	324
Panofsky ratio I	11013	C-3	H_2	36.85	7051	6922	1437	1685	219	564 (low) 8 (high)	21	87.5 to 131.5	2475	513	2988	7057
Panofsky ratio I	11013	out	H_2	15.63	190	164	34	56	3	13 (low)		87.5 to 131.5	51	7	58	130
Panofsky ratio II	8235	C-2	H_2	56.31	11376	11196	1682	3847	362	60 (between) 4 (high)	51	51.4 to 83.5	3445	503	3948	17929
												90.5 to 130.5	959	283	1242	6385
Panofsky ratio II	8235	out	H_2	30.33	485	440	57	192	17	2 (between)	3	51.4 to 83.5	106	24	130	573
												90.5 to 130.5	27	12	39	210
Deuterium ratio S	10500	C-3	H_2	992.8	8517	8401	1673	1931	347	1062 (low) 6 (high)	14	88 to 132	2787	580	3367	7542
Deuterium ratio S	10500	C-3	D_2	1057.2	3916	3831	380	822	201	77 (low) 4 (high)	8	88 to 132	1987	352	2339	5320

E and $E+\Delta E$ is

$$P(E)\Delta E=\gamma(T)S(T,B)\int^{E_\gamma} I(E_\gamma)R(E_\gamma,E)dE_\gamma\epsilon(E)\Delta E), \quad (16)$$

where $\gamma(T)$ is the probability for pair production in the converter averaged over the spectrum of incident energies, $S(T,B)$ is the probability that the vertical positions for both particles at the 180-deg orbit positions are within the detector vertical limits, and $R(E_\gamma,E)$ is the resolution function that describes the energy distribution of pairs emerging from the converter. The lateral-detection efficiency $\epsilon(E)$ specifies the fraction of pairs with total energy E for which both particles enter the lateral limits of the detectors. The integration extends over all γ-ray energies occurring in the distribution $I(E_\gamma)$.

A. The Resolution Function $R(E_\gamma,E)$

This function is defined as

$$R(E_\gamma,E)=\int^{E_0^-} p(E_\gamma,E_0^-)\int_0^T W(E_\gamma,t,B)\times\int^{E_1^-} F^-(E_\gamma,t,E_0^-)\times F^+(E_\gamma-E_0^-,\, t,\, E-E_1^-)dE_1^-dtdE_0^-, \quad (17)$$

where the integrations extend over all values of the initial and final electron energies, E_0^- and E_1^-, and where $\int_0^{E_\gamma}R(E_\gamma,E)dE=1$. The function $p(E_\gamma,E_0^-)$ denotes the distribution of electron energies occurring in pair production. The function $W(E_\gamma,T,B)$ serves to weight slices of the converter with respect to pair-production yield and scattering losses. For given initial particle energies and position in the converter, the functions F^- and F^+ describe the distribution in final electron and positron energies, E_1^- and $E-E_1^-$, upon the particles leaving the converter. These latter functions include contributions to the energy loss from bremsstrahlung (or radiation straggling) and ionization as well as the line broadening resulting from the Geiger-tube channel width. In the calculation of the resolution these three effects are treated separately and the resulting distributions folded together.

We calculated the channel-width distribution by folding together two uniform distributions both of energy width equal to a Geiger channel, one corresponding to the electron side of the spectrometer, the other to the positron side. The result of this fold is an equilateral triangle with base width equal to the sum of the channel widths. For a magnetic field setting of 10 500 G the channel width is 1 MeV.

For ionization-energy losses, the Landau[24] distribution is used with the most probable energy loss corrected for the density effect as described by Sternheimer.[25] Because of the independence of ionization-energy loss with electron energy, the energy-loss distribution for the pair was calculated by averaging the Landau distribution for an electron over twice the thickness of the actual converter. In the averaging process the tails of the Landau distribution for each converter slice were extended to an energy E' where, in the averaged distribution, less than 1.5% of the pairs had energies less than E'.

[24] L. Landau, J. Phys. (U.S.S.R.) 8, 201 (1944).
[25] R. M. Sternheimer, Phys. Rev. 103, 511 (1956).

The radiation straggling distributions for electrons and positrons are computed using the sum of the cross sections from bremsstrahlung in the field of the nucleus as derived by Davies, Bethe, and Maximon,[26] and the cross sections for bremsstrahlung in the field of the atomic electrons as given by Wheeler and Lamb.[27] To obtain the integrated radiation straggling as a function of total pair energy, we integrated the individual electron and positron radiation distributions over final electron energy, converter thickness, and initial electron energy as indicated in Eq. (17). The IBM 709 computer was programmed for this calculation.

B. Lateral-Detection Efficiency

The lateral-detection efficiency $\epsilon(E)$ is determined by the counter geometry, by the pair-fragment energy distribution $p(E_\gamma,E_0^-)$ for the incident γ ray, and by the energy-loss distributions of the electron and positron. Since the values of $p(E_\gamma,E_0)$ for the range of particle energies detected by the spectrometer are quite close to the average value, and because the converters are thin, $\epsilon(E)$ can be determined to within a few percent of its correct value by geometry considerations alone. Because $\epsilon(E)$ is dependent upon γ-ray energy, the measured data are corrected to first approximation for the energy dependence of the detection system using $\epsilon(E)$, determined as above. The necessary correction factor is, then, evaluated by use of the computer program mentioned in Sec. VA.

VI. DATA AND ANALYSIS

A. Treatment of Data

In scanning the film we identified for each event all neon lamps that fired by the numbers of the corresponding Geiger tubes and scintillators. The difference between the numbers representing the positron- and electron-detector channels, which is directly proportional to the distance between detectors, was then converted into total pair energy. A summary of the data is presented in Table II.

The difference between the "Total gates" and "Total events recorded" columns in Table II is due primarily to accidental coincidences of the gate counters for which no γ ray is involved.

For geometrical reasons a few channels in the spectrometer detection array were not used. The limits of the useful region are indicated in Fig. 4 by the minimum and maximum orbits. Events in which either the electron or positron falls outside this region were rejected. The number of these is given under Column A in Table II. Additionally, for each measurement, the data analysis was performed over a limited range of energies (Column $E_A \rightarrow E_B$) of the detected pairs. Events falling outside this range are noted in Column D. Because of the relatively small variations in efficiency of the Geiger tubes (see Sec. III C) and because, in general, many different pairs of electron and positron channels correspond to the same energy, it is assumed that the Geiger-tube efficiency, averaged over all constant-energy channels, is independent of total pair energy. Therefore, it is permissible to reject all events in which Geiger tubes on one or both sides do not fire. The number of these events is given under Column B. Since the efficiency of the channel scintillation counters is quite large (>97% for each electron or positron channel) and since in general several sets of electron and positron channels correspond to the same energy, it is also assumed that the efficiency of the scintillation-counter system is independent of total pair energy. To eliminate any possible energy-dependent background, all scintillators overlapping the firing Geiger-tube channel were also required to fire. The number of events not meeting this requirement is given in Column C.

Acceptable events are classified as "good" or "extra." "Good" events are those for which either one Geiger tube or two overlapping ones fire on both electron and positron sides and for which the overlapping scintillator-channel counters all fire. "Extra" events are those in which additional Geiger tubes fire and for which the scintillator and Geiger channels are in agreement. Since several of the processes which cause extra Geiger tubes to fire are energy dependent, it is necessary that these events be included.

In approximately 80% of the extra events less than 4 Geiger tubes fire on either side. For a large majority of these events the energy could be determined to within one or two Geiger channel widths. However, in nearly all cases the γ-ray group involved could be determined.

The "uncertain events" in Table II are events in which extra Geiger tubes fire and for which either the γ-ray group involved could not be determined or we could not ascertain whether the incident electron or positron passed through the acceptable detector channels. If these events are equally divided among the possible alternatives, no significant influence on the ratios being measured results. Since the number of these events is small, we have chosen to ignore them.

Let a number of γ rays, N_γ, be incident upon the converter. If $n_d(\Delta E)$ is the number of pairs detected in an energy channel of width ΔE, then

$$N_\gamma = n_d(\Delta E)/P(E)\Delta E, \tag{18}$$

which, by substituting Eq. (16) for $P(E)\Delta E$, can be rewritten as

$$N_\gamma = \frac{n_d(\Delta E)}{\epsilon(E)} \Big/ \gamma(T)S(T,B) \times \int^{E_\gamma} I(E_\gamma)R(E_\gamma,E)dE_\gamma \Delta E. \tag{19}$$

[26] H. Davies, H. A. Bethe, and L. C. Maximon, Phys. Rev. **93**, 788 (1954).

[27] J. A. Wheeler and W. E. Lamb, Phys. Rev. **55**, 858 (1939) with correction in Phys. Rev. **101**, 1836 (1956).

Since N_γ is independent of the energy interval over which the measurement is made, for an interval between E_A and E_B we can write

$$N_\gamma = N_d/\gamma(T)S(T,B)\Sigma \tag{20}$$

where

$$\Sigma = \sum_{E_A}^{E_B} R(E)\Delta E = \sum_{E_A}^{E_B} \int^{E_\gamma} I(E_\gamma)R(E_\gamma,E)dE_\gamma \Delta E \tag{21}$$

and

$$N_d = \sum_{E_A}^{E_B} N_d(\Delta E) = \sum_{E_A}^{E_B} \frac{n_d(\Delta E)}{\epsilon(E)}; \tag{22}$$

the numerical values of N_d are given in Table II for the various measurements.

The γ ray yields obtained for each converter with the H_2 removed from the target were approximately 0.5% of the corresponding yields with the H_2 in. This is consistent with the assumption that this yield is entirely due to interactions of the π^- mesons with the residual H_2 gas in the target.

It can be seen from Table II, Column D, that for the radiative-capture reaction the number of events detected with energies larger than the high-energy cutoff E_B is quite small. Although some of these events may be due to accidental background, the numbers are consistent with what is expected from radiative capture in flight. Since the detectable energy range above E_B is in general quite appreciable, the accidental background is assumed negligible.

B. Spectrometer Performance Checks

Several checks were made to ensure that the spectrometer operation was as predicted. With the spectrometer field set at 10 500 G the yield from the radiative-capture reaction in hydrogen was measured for several converter thicknesses. The "scattering in" probability $S(T,B)$ for each thickness was then determined according to Eq. (20). The results are presented in Fig. 5. The solid curve in the figure represents the results of a theoretical calculation of $S(T,B)$ in which for the projected angle the Gaussian part of the Moliere scattering distribution was used.

The measured ratio of yield with converter in to yield with converter out for the Panofsky ratio runs was compared with that calculated using Eq. (20). The results of this comparison are reasonable and provide good evidence that only pairs created in the converter are detected.

Since the number of γ rays incident upon the converter, N_γ, is independent of magnetic field, a comparison of measured values of N_γ for the same γ-ray spectra but different fields provides a check on any magnetic-field effects. We determined N_γ from Eq. (20) using the Panofsky ratio data. For the mesonic capture γ rays, the ratio of N_γ, as determined from the results at the medium field, to N_γ, as determined at the low field, is 0.999 ± 0.043. The corresponding ratio for the radiative-capture γ rays at the medium and high fields is 0.948 ± 0.041.

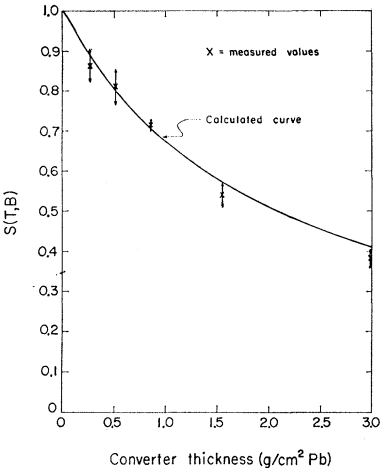

FIG. 5. "Scattering in" probability $S(T,B)$ vs converter thickness for $B=10{,}500$ G.

C. Panofsky Ratio Calculation

The measured Panofsky ratio, formula (12), can be rewritten in terms of Eq. (20) to give

$$P = (MC'C''C''')\frac{N_{d1}}{2N_{d2}}\frac{\gamma_2(T)}{\gamma_1(T)}\frac{S_2(T,B)}{S_1(T,B)}\frac{\Sigma_2}{\Sigma_1}. \tag{23}$$

Subscripts 1 and 2 refer to the mesonic-capture and radiative-capture γ rays, respectively. The factor M normalizes the yields from the two reactions to the same number of π^- mesons stopping in the target. The C', C'', and C''' are correction factors; C' compensates for the inexact lateral-detection efficiency used in evaluating N_d (see Sec. V), C'' adjusts the data for the internal-conversion reactions, and C''' corrects the measured mesonic-capture spectrum for the contribution resulting from radiative-capture γ rays.

We have corrected for the effect produced by the converter counter by subtracting the measured γ-ray yield with converter out from the yield with converter in.

With the pair spectrometer, electrons produced by γ-ray Compton scattering in the converter are not detected. Considering this, the probability for pair production in the converter is given by

$$\gamma(T) = \frac{\sigma_p}{\sigma_p+\sigma_c}(1-e^{-\rho(\sigma_p+\sigma_c)T}), \tag{24}$$

where ρ is the density and σ_p and σ_c are the cross sections for pair production and Compton scattering, respectively, averaged over the energy spectrum considered. The sum of the cross sections for pair production in the field of the nucleus and the field of the atomic electrons is used. For the nuclear contribution the results

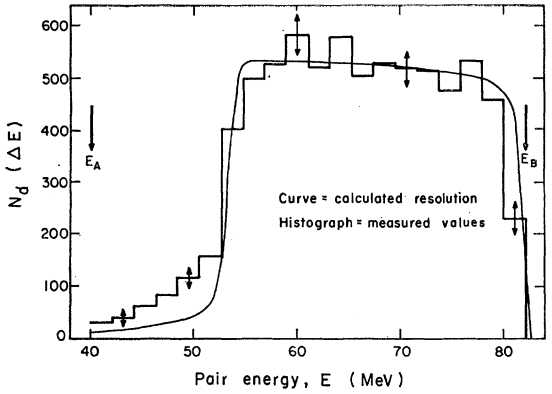

FIG. 6. Mesonic-capture γ-ray spectra for $B=5{,}538$ G and converter C-1.

of Davis, Bethe, and Maximon[26] are employed with an energy-dependent correction factor as discussed in National Bureau of Standards Circular 583. The contribution by the atomic electrons is determined from the results of Vortruba.[28] For the Compton scattering cross section the Klein-Nishina formula is used. The values of the ratios $\gamma_2(T)/\gamma_1(T)$ calculated for measurements I and II are 3.720 ± 0.038 and 1.147 ± 0.012, respectively.

Although the thicknesses of the converters were selected to equalize the "scattering in" probability $S(T,B)$ for each field setting, the thickness of converter C-1 deviates slightly from the required value. The correction for this was determined from Fig. 5. The resulting value for the ratio $S_2(T,B)/S_1(T,B)$ for measurement I is 0.996.

The calculated spectra $R_1(E)$ and $R_2(E)$ [$R(E)$ is generally defined in Eq. (21)] are shown in Figs. 6 and 7, respectively, for measurement I, and Fig. 8 for measurement II. The corresponding measured spectra are also given. Since the energy scales of the calculated spectra are absolute, the curves were fitted to the measured data merely by adjusting the heights. For the radiative-capture γ ray the calculated spectra was adjusted so that the areas in the peak between 124 and 130 MeV for both spectra were equal. The limits of the energy intervals over which N_d and Σ have been evaluated are indicated in these figures by arrows.

We note in Figs. 6, 7, and 8 that the calculated spectra are consistently smaller in the tails than the measured spectra. Possible reasons for this are discussed in Sec. VII. Because of this effect there is some uncertainty in determining the quantities Σ_1 and Σ_2. If we assume that the discrepancy results from an incomplete accounting of bremsstrahlung, then, since the tails of the calculated spectra are almost entirely due to bremsstrahlung, a correction to the calculated value for Σ is obtained by taking the relative discrepancy as constant from the lower cutoff energy down to zero. The value of Σ obtained in this manner is considered a lower limit. If the discrepancy is caused by other energy-loss effects, such as ionization, it is believed the tail contribution would not be as great. Since the behavior in the tail is not known, the value of Σ calculated from theory is taken as the upper limit. The upper and lower limits for Σ_1, Σ_2, and the ratio Σ_2/Σ_1 derived from this analysis are tabulated as follows:

	Measurement I		Measurement II	
	Upper limit	Lower limit	Upper limit	Lower limit
Σ_1	0.991	0.978	0.963	0.907
Σ_2	0.950	0.913	0.970	0.948
Σ_2/Σ_1	0.959	0.934	1.007	1.045

It is now assumed that the correct value for the ratio Σ_2/Σ_1 lies with equal probability anywhere between the upper and lower limits.

The factor C'' adjusts the measured data so that the results for P are expressed in terms of the definition in Eq. (4), where

$$P=\frac{(1a)+(1b)}{(2)+(3)}. \tag{4}$$

In the present method of measurement, Reaction (1b) is detected only half as efficiently as (1a) while Reaction (3) is never detected; C'' is calculated to be

$$C''=\frac{1+j}{(1+j')(1+j/2)}, \tag{25}$$

where j is the branching ratio (1b)/(1a), and j' is the ratio (3)/(2). Using the values for these ratios given in the Introduction, C'' is determined to be 0.999.

Finally the values obtained for P from Eq. (23) are 1.490 ± 0.050 for Measurement I, and 1.543 ± 0.063 for Measurement II.

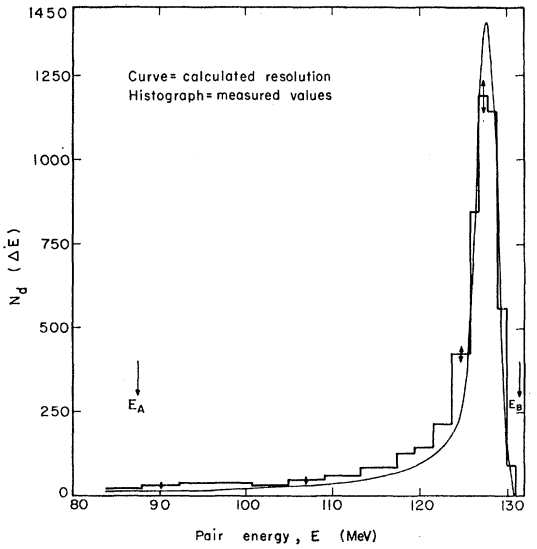

FIG. 7. Radiative-capture γ-ray spectra for $B=11\,013$ G and converter C-3.

[28] V. Vortruba, Phys. Rev. **73**, 1468 (1948).

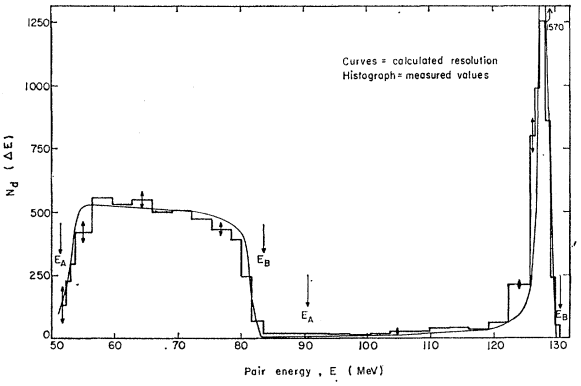

FIG. 8. Mesonic-capture and radiative-capture γ-ray spectra for $B=8235$ G and converter C-2.

D. Deuterium Ratio S Calculation

The measured deuterium ratio, formula (15), written in terms of Eq. (20) is

$$S=\left[M(1+p)\frac{N_{d2}}{N_{d4}}\frac{\gamma_4(T)}{\gamma_2(T)}\frac{\Sigma_4}{\Sigma_2}\right]-1. \tag{26}$$

Subscripts 2 and 4 refer to the hydrogen and deuterium radiative-capture reactions, respectively. The ratio of the term in Eq. (20) involving $S(T,B)$ is unity and is omitted in Eq. (26). Additionally, corrections to the measured spectra due to the lateral detection efficiency are nearly identical and no adjustment to S is necessary.

Spectrographic analysis of the deuterium used in the experiment indicated a 2.25% contamination of hydrogen. In correcting for the effects of this, we assume that the yield due to the hydrogen is directly proportional to the concentration of hydrogen. Calculations made by Cohen, Judd, and Riddell[29] for μ^- mesonic-atom systems indicate that for a μ^-p atom moving with low energy through pure deuterium the rate for transfer of the μ^- meson to a deuterium atom is $\approx 10^{10}$ sec^{-1}. However, the rate for nuclear capture of a π^- meson from a π^-p mesonic-atom state is $>25\times 10^{10}$/sec.[30] Since it is reasonable that the probability for capture of a π^- meson into a π^-p mesonic-atom state is proportional to the concentration of hydrogen and that the above transfer rate is not very different for the π^- meson, our assumption is justified. The correction was made by subtracting from the measured deuterium yield the contribution due to the hydrogen contamination and then adding that contribution which would have resulted if the hydrogen had been deuterium.

The pair-production probability for the deuterium γ-ray distribution, $\gamma_4(T)$, was calculated by using an average value for the cross section weighted in terms of the γ-ray distribution. The assumed form of the distribution was taken from the calculations of Watson and Stewart[31] for a value of the n-n scattering length as determined by Crowe and Phillips.[32] The value obtained for the ratio $\gamma_4(T)/\gamma_2(T)$ is 0.995.

To evaluate the ratio Σ_4/Σ_2, the relative contributions in the tails of the measured spectra below the low-energy cutoff must be determined. The measured distributions $N_d(\Delta E)$ for both the H_2 and D_2 γ rays are shown in Fig. 9 where the distributions have been normalized to the same number of events. The cutoff energies are indicated by arrows. Since most of the contribution in the tail of the hydrogen distribution is due to radiation straggling, the contribution in the deuterium tail should be approximately 20% larger due to enhanced contributions from lower energy γ rays. After taking this into account we linearly extrapolated the difference remaining in the two spectra at the lower cutoff energy to zero energy. A contribution of 2.7% of the total spectra was obtained. Since the shape of actual deuterium γ-rays spectrum is expected to fall off with decreasing energy faster than linearly, the value for this contribution is taken as 1.4 ± 1.0. The ratio Σ_4/Σ_2 was calculated using this procedure for both the upper and lower limits of Σ_2 as determined in the manner discussed in Sec. VI C. The two results were averaged together to give

$$\Sigma_4/\Sigma_2=0.97\pm 0.01.$$

In the normalization term, M, it is necessary to include in addition to the ratio of monitor counts a factor which compensates for the difference in stopping power between H_2 and D_2. The average ionization-energy loss for heavy charged particles can be written as

$$\frac{dE}{dx}\approx\frac{\rho Z}{Av^2}f(v,\bar{I}). \tag{27}$$

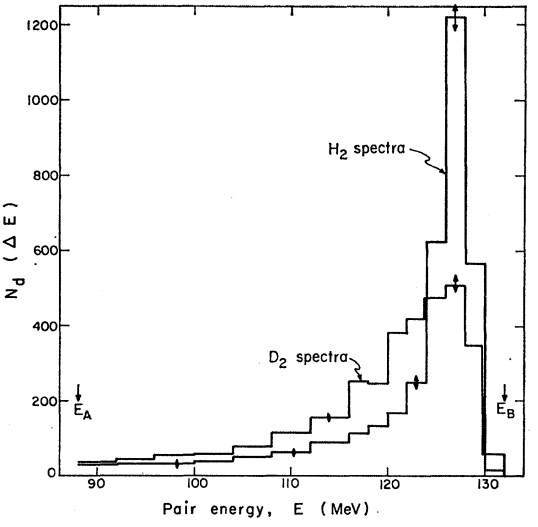

FIG. 9. Measured radiative-capture γ-ray spectra for H_2 and D_2 ($B=10{,}500$ G).

[29] S. Cohen, D. L. Judd, and R. L. Riddell, Jr., Lawrence Radiation Laboratory Report UCRL-8391, 1959 (unpublished).
[30] J. Fields, G. B. Yodh, M. Derrick, and J. Tetkovich, Phys. Rev. Letters **5**, 69 (1960).
[31] K. Watson and R. Stuart, Phys. Rev. **82**, 738 (1951).
[32] R. H. Phillips and K. M. Crowe, Phys. Rev. **96**, 484 (1954).

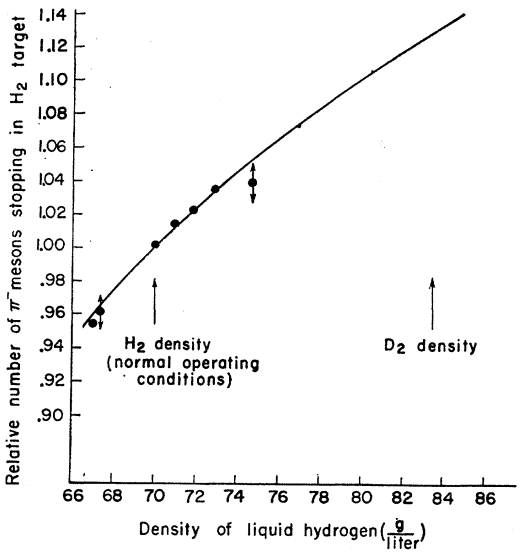

FIG. 10. Relative number of π^- mesons stopping in the hydrogen target vs hydrogen density.

Now Z is the same and $\bar{I}$ nearly so for both H_2 and D_2. However, ρ/A for D_2 is nearly 15% larger than for H_2 and hence the stopping power 15% larger. However, since the energy spectrum of the π^- beam was not uniform, it was necessary to determine experimentally the relative number of π^- mesons stopping in the H_2 and D_2. Two independent methods are employed.

In the first method, the γ-ray telescope counting rate as a function of energy-degrader thickness is measured with H_2 in the target. By using the known H_2 target thickness, this curve is unfolded to yield the range distribution of the incident π^- meson beam. Knowing the beam-range distribution, we can obtain the relative number of π^- mesons stopping in the target as a function of H_2 density. The results are shown by the smooth curve in Fig. 10. The normal density of the hydrogen and the density corresponding to the same stopping power as the deuterium are both indicated.

In the second method, we obtain several different values of hydrogen density by suitably pressurizing the liquid-hydrogen system (see Sec. IV). By monitoring the reaction rate with the γ-ray telescope, we determine the relative π^- meson stopping rate as a function of density. The measured values are shown in Fig. 10. The ratio of the number of π^- mesons stopping in the D_2 target to the number stopping in the H_2 target as a result of the stopping power difference is determined from Fig. 10 to be 1.13. Using Eq. 26 the value we obtain for the deuterium ratio S is 3.16 ± 0.12.

E. Error Analysis

In evaluating the errors for P (Measurements I and II) and for S, we treat the errors on the quantities in Eq. (23) and (26) as independent and standard. The errors on the ratios involving N_d are purely statistical and have been determined by the usual method of error propagation for independent errors.

Due to the relatively small background in the γ-ray monitor-telescope counting rate, the accuracy of this monitor is limited by fluctuations in losses in the scaling system. These fluctuations are less than 2%. A comparison of the two monitoring systems used shows that the average fluctuations in the relative indications are of this same magnitude. Since more than 15 runs were performed for each converter-field situation and since the various types of runs alternated, we estimate the monitoring error to be 0.3%. For the Panofsky-ratio measurement this is the only source of error in the normalization factor M. However, for the deuterium-ratio S measurement, an additional 1% error has been assigned to M due to the difference in stopping power of the π^- mesons in H_2 and D_2. This error arises from the uncertainty in the range curve unfolding.

Since the pair-production probabilities $\gamma(T)$ are small compared to one, we can write

$$\gamma(T) \propto 1-e^{-\rho\sigma T} \approx \rho\sigma T.$$

Therefore, the fractional error in the ratio of probabilities is just the fractional error in the ratio of cross sections. The errors in the cross sections arise from the approximations made in the calculations of Bethe, Davis, and Maximon.[28] Since the ratio only is involved here, the error should be small. We estimate a 1% error in the ratio for the Panofsky ratio results.

In addition to the errors on the quantities in Eq. (26), a 1.3% error has been included to account for the uncertainty in the relative positioning of the H_2 and D_2 targets (see Sec. III B).

VII. RESULTS AND DISCUSSION

The final results for the Panofsky ratio and the deuterium ratio S are

$$P=1.51\pm0.04,$$

and

$$S=3.16\pm0.12.$$

Here P is the weighted average of the values determined for Measurements I and II in Sec. VI C. Previous measurements of P are shown in Table I. If each of these is weighted according to the quoted error, the value obtained is

$$P=1.54\pm0.02.$$

Our result is in complete agreement.

The value of S obtained here is significantly higher than the results of previous measurements or that calculated from Eq. (11) (see Table I). Although the reason for this disagreement is not known, systematic errors on this measurement are believed to be quite small since the same converter and the same magnetic field are used for both the hydrogen and deuterium runs, and since both radiative-capture γ-ray spectra are quite similar.

As indicated in Sec. VI C, a discrepancy exists between the shape of the theoretical spectra and the measured spectra. The values determined for P and S depend upon the assumed cause of this discrepancy. In obtaining the above results, we have assumed that the discrepancy is caused by energy losses of the electrons and positrons in the converter being incompletely accounted for. In the following paragraphs we discuss the various possible causes of this effect and the probable magnitudes of their contributions. These include (a) reduced energy γ rays entering the spectrometer, (b) apparent or real energy-loss effects associated with the spectrometer design, and (c) uncertainties in the energy loss of high-energy relativistic electrons.

The first possible cause might involve either nuclear reaction in which lower energy γ rays are produced or γ rays with reduced energy produced by the Compton effect or by the shower formation on the collimator walls. It is noted that the measured hydrogen radiative-capture spectrum can be reconstructed very well with a combination of 82% of the theoretical hydrogen spectra plus 18% of the measured deuterium spectra. Since the hydrogen used had the normal isotopic abundance, then, if this apparent agreement were meaningful, it would imply a very high transfer rate of the π^- meson between hydrogen and deuterium. However, as indicated in Sec. VI D the transfer rate even in pure deuterium is believed to be relatively small. This small transfer rate, together with the fact that the π^0 γ-ray spectra also display a similar effect, leads us to consider this explanation as quite improbable. Rough calculations of Compton scattering of γ rays in the collimator walls indicate the contribution of reduced energy γ rays due to such scattering should be much smaller than the observed effect. It seems unlikely that Compton scattering or shower formation would yield a γ-ray spectrum required to explain the discrepancy. However, if Compton scattering on the collimator walls were assumed to be the cause, from a comparison of the measured and theoretical spectra it is estimated that the quoted value for P would be reduced by 6% and S would remain essentially unchanged. This reduced value for P, however, would disagree significantly with previous measured values of P.

With respect to energy-loss effects due to spectrometer design, an electron undergoing a large-angle scattering in the converter may enter the detector region with apparent lower energy. For an apparent energy decrease of a few MeV it is very probable that several Geiger tubes would be triggered and the event classified as "extra," as defined in Sec. VI A. However, the measured spectra are essentially the same whether these events are included or not. The scattering calculations also indicate that these large-angle scattering events are too rare to explain the observed effect; they also indicate that the number of electrons scattered off the pole tip or the Geiger holders and back into the detector region thus simulating a reduced-energy electron, is much too small to account for the observed results.

There are two processes by which the electron and positron can lose energy in the converter: bremsstrahlung and ionization. The bremsstrahlung cross section employed (see Sec. VI C) is believed to be accurate to within a few percent, but has not been experimentally verified. A summary of previous bremsstrahlung measurements is given in the review article by Koch and Motz.[33] With respect to ionization, the Landau-ionization energy-loss distribution for high-energy electrons has been checked by Hudson[34] who obtains slight deviations in the shape of the distribution near the high-energy end and excellent agreement with respect to the most probable energy loss. However, very little experimental information is available with regard to the tail of the distribution.

[33] H. W. Koch and J. W. Motz, Rev. Mod. Phys. **31**, 920 (1959).
[34] A. M. Hudson, Phys. Rev. **105**, 1 (1957).